ACS Energy LETTERS

http://pubs.acs.org/journal/aelccp

Technoeconomic Model Suggests Scaling-Up Perovskite Quantum Dots for Optoelectronics Warrants Improved Synthesis Yield, Solvent Recycling, and Automation

Cite This: *ACS Energy Lett.* 2022, 7, 1255−1259 Read Online

ACCESS | Metrics & More | Article Recommendations | Supporting Information

Colloidal quantum dots (QDs) are nanometer-sized semiconductor crystals grown via low-cost solution processing routes for a wide array of applications encompassing photovoltaics, light-emitting diodes (LEDs), electronics, photodetectors, photocatalysis, lasers, drug delivery, and agriculture.[1−3] Perovskite nanocrystals are an emerging class of QDs that exhibit remarkable defect tolerance, leading to the best-in-class QD-based photovoltaics and materials for lighting/display applications.[3,4] Cesium lead halide ($CsPbX_3$, X = I, Br, Cl) QDs are particularly attractive for optoelectronics, and $CsPbI_3$ QDs have been extensively explored as solar cell absorbers, given their suitable bandgap (1.74 eV) and high photovoltages.[5] While halide perovskite solar cells do not necessitate perovskite quantum dots (PQDs), and in fact there is significantly more research ongoing for thin film perovskites using other deposition methods, a cost model for the production of PQDs at this stage becomes useful as concepts are still being developed. PQDs have characteristics not examined in other models such as crystallization as an ink, rather than on device substrates, and the intrinsic benefit of lattice-strain-induced phase stability.[6]

PQDs are synthesized by employing a commonly used "hot-injection" method where one precursor is swiftly injected into another at an elevated temperature, along with surface ligand molecules.[7] The size of the QDs is mainly defined by the solution temperature but could be controlled by other parameters such as precursor ratio or ligand concentration. The resulting QDs in 1-octadecene (ODE) are then purified via multiple centrifugation steps using methyl acetate (MeOAc) and hexane, eventually resulting in an optoelectronic-grade QD colloid in octane that can be deposited to form thin films for optoelectronic devices. The ionic nature of PQDs necessitates capping them with long-chain ligands and dispersing in a nonpolar, organic solvent. Since a robust solution-phase ligand exchange to improve the conductivity of PQD films does not yet exist, the absorber layer fabrication is done using a layer-by-layer (LbL) film-based ligand exchange.[1,8] Films formed from organic-capped QDs are exposed to MeOAc, followed by a treatment with formamidinium iodide (FAI) to strip off the organic ligands and bring the QDs closer for increased electrical conductivity.[9,10]

In this Energy Focus, we present a comprehensive technoeconomic cost analysis of PQD synthesis, considering $CsPbI_3$ as a model system, including economies-of-scale (EoS) considerations based on price data gathered from prominent materials suppliers. The analysis highlights that the current synthesis protocol is highly cost-inefficient and incompatible with industrial scale-up. *Increased QD synthesis yield*, *solvent recycling*, and *synthesis automation* are suggested as key enablers of cost competitiveness. These recommendations are generic and should apply to all colloidal QD compositions vying for market entry that suffer from a low synthetic yield and high labor costs.

A typical synthesis batch of $CsPbI_3$ QDs requires swift injection of a small amount of Cs-oleate solution into a heated flask containing 500 mg of PbI_2 dissolved in 25 mL of ODE, as has been detailed earlier.[5,10] The resulting QDs are separated via centrifugation, washed, and dispersed in octane for optoelectronic film fabrication. Usually, 60 mg of optoelectronic-grade, high-quality QDs can be recovered from one such batch.[5,11] Loosely bound surface ligands can result in synthesis yield loss during centrifugation. Also, the synthesis is dictated by cesium carbonate (Cs_2CO_3), being the limiting reagent. An excess of PbI_2 has been traditionally required for nucleation and growth of high-quality $CsPbI_3$ QDs, and therefore Cs_2CO_3 is completely consumed during the reaction.[7,12,13] Since PbI_2 is the major component of this reaction and most of it is wasted, for this analysis we define QD synthesis yield (Y) as the ratio of the final optoelectronic-grade QDs' mass to the PbI_2 mass. Common QD reactions have a Y of ∼12%.

$$Y\ (\%) = \frac{\text{mass of optoelectronic-grade QDs}}{\text{mass of PbI}_2} \times 100\%$$

Received: January 31, 2022
Accepted: February 25, 2022

ACS Publications Published XXXX by American Chemical Society

https://doi.org/10.1021/acsenergylett.2c00250

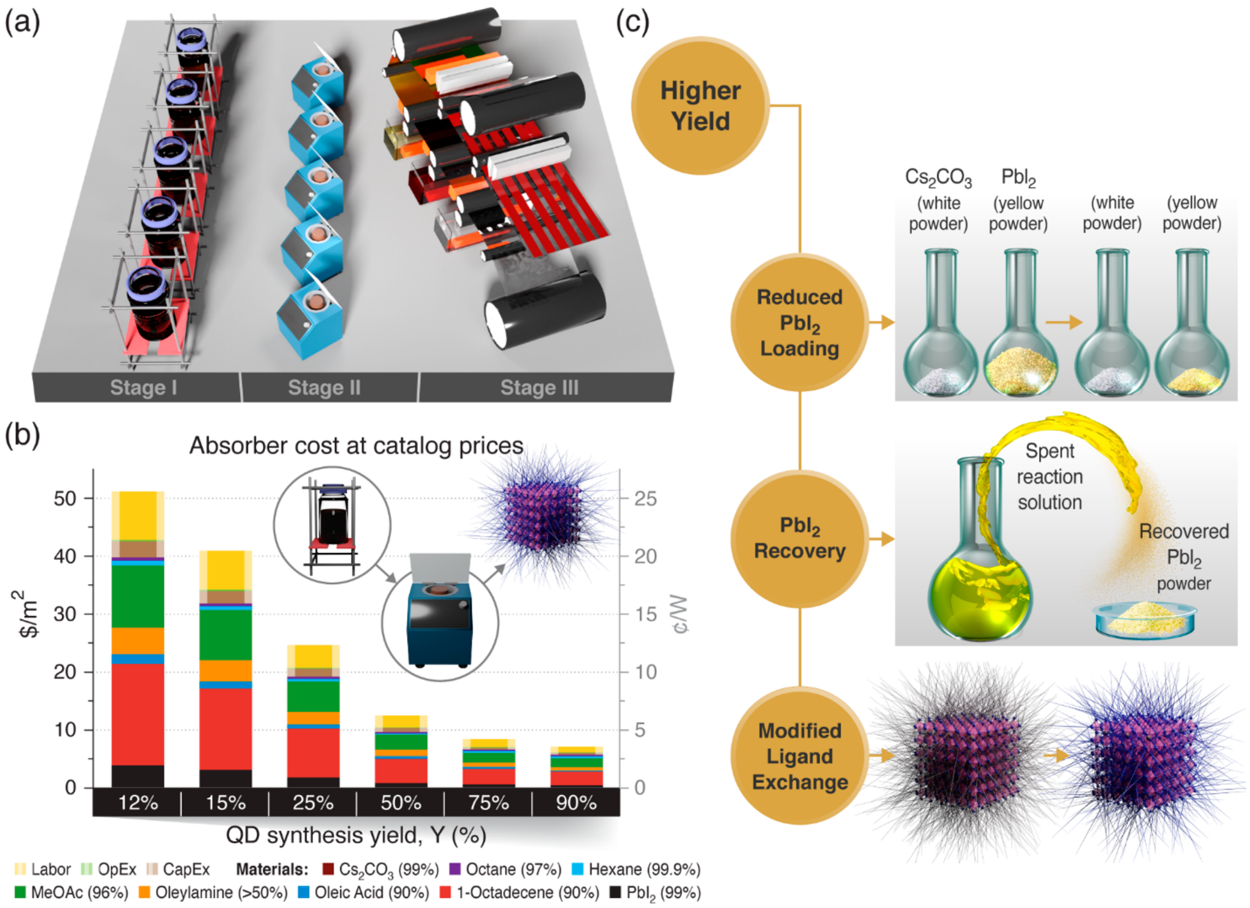

Figure 1. Effects of synthesis yield. (a) Schematic depicting the various scale-up stages for PQD optoelectronics: synthesis (Stage I), cleaning (Stage II), and roll-to-roll (R2R) coating (Stage III). (b) Catalog pricing-based \$/m^2 for QDs as a function of synthesis yield (Y) for small-scale photovoltaic (PV) production. The purity of the various precursors and solvents is denoted in parentheses in the legend and is based on literature reports.[5,10] (c) Potential routes to achieving higher synthesis yields from the hot-injection method.

It is important to note that, although the loose binding of ligands to PQDs reduces Y, it is required for ease of film formation since only nonpolar solvents can be used during the ligand-exchange step, which are not very efficient in ligand exchange. This is clear from the case of cesium lead bromide ($CsPbBr_3$) QDs, where organic ligand binding is much stronger, resulting in high PLQY and Y; however, fabrication of thicker absorber layers (~200 nm thickness) is challenging.[14] The current synthesis routes for PQDs therefore present a trade-off between Y and manufacturability. This is in contrast with the case of metal chalcogenide QDs, where ligand binding is strong, resulting in significantly higher Y. Since these QDs are not as ionic, polar solvents such as methanol and acetonitrile along with thiol linkers are usually used for ligand exchange, enabling efficient ligand stripping and film fabrication.[1,15−18]

Impact of QD Synthesis Yield (*Y*). As discussed above, lower Y for $CsPbI_3$ QDs can be attributed to two causes: the need for a significantly Pb-rich environment during synthesis and loss during cleaning due to loosely bound ligands. There have been recent attempts to circumvent the loss related to the cleaning stage. Efficient ligand exchange was realized by incorporating a secondary amine into MeOAc, leading to higher Y (= 40%) and notable solar cell device performance.[11]

Figure 1a shows the three stages involved in PQD solar cell fabrication in a pilot manufacturing facility. Stage I involves hot-injection PQD synthesis, and Stage II deals with cleaning. The cleaned optoelectronic-grade PQDs are then transferred to a roll-to-roll (R2R) coating system for module fabrication (Stage III). The capital expenditure (CapEx), operational expenditure (OpEx), and labor charges were defined considering Pb and Cs reaction vessels (10 L reaction volume) for Stage I, large-volume continuous-flow centrifuges for Stage II that can handle 400 L of QD colloid in 24 h, and an equipment lifetime of 5 years. The lifetime of the factory building was assumed to be 20 years. An equipment-to-employee ratio of 1 was considered, and standard U.S. labor rates of \$27/h for the employees and \$36/h for the supervisors (1 per every 5 employees) were used. A flowchart describing the various steps in this cost model is shown in the Supporting Information (SI), Schematic S1.

Figure 1b shows the impact of Y on the cost of active-layer fabrication. Cost is normalized to a unit area of coated film (\$/m^2), assuming that 1 g of synthesized optoelectronic-grade QDs can be deposited over 1 m^2 substrate.[19] Please see the associated detailed discussion in the SI regarding the 1 g/m^2 assumption and the precursor and solvent cost calculations based on catalog pricing (Table S1). The low g/m^2 requirement is a likely scenario given recent demonstrations of blade-coated QD optoelectronic devices that have required significantly lower volumes of the QD ink compared to spin-coating.[19−21] For photovoltaic (PV) applications, \$/m^2 can then be converted to cost-per-watt (\$/W) power generated, assuming a module with 20% power conversion efficiency (PCE), as highlighted in Figure S1a. In this cost model, \$/W is calculated considering the initial output power. Module lifetime is an input needed to calculate the levelized cost of energy (LCOE), but the lifetimes of many next-generation PV technologies, including PQDs and perovskites, are not yet well established. It has been suggested that a significantly lower module lifetime of 10 years for a thin film PV technology (as opposed to 25 years for existing technologies) can suffice for market entry, given the ease of device assembly and the anticipated improvements achievable in the near term.[22] Due to these complications, we have not considered LCOE in this cost model. Furthermore, \$/m^2 captures cost investment for multiple next-generation technologies using PQDs including LEDs and displays, radiation detectors, lasers, and spectrum-shifting QD films for either PV or agriculture.

The \$/m^2 values shown in Figure 1b are for the PQD active layer; costs related to the substrate, electrodes, charge contact layers, balance-of-module, etc. are not considered for simplicity. The overall cost is a sum of the materials expenditure, CapEx, OpEx, and labor charges. Further, materials expenditure is based on catalog prices of the various precursors and solvents available on vendor Web sites for the maximum volumes purchasable. It is important to note that the cost component from factors other than the active layer (substrate, electrodes, charge contact layers, balance-of-module, etc.) largely remains independent of the absorber layer technology and can be assumed to be \$35/m^2 following a recent comprehensive analysis for hybrid organic–inorganic perovskite photovoltaics.[23] This simplification allows us to focus on the active layer cost optimization. A comparison with the established Si PV industry suggests that, for a thin-film optoelectronics technology to be market-compatible, the active layer cost should be < \$5/m^2, resulting in a \$/W value of <0.20, considering 20% PCE modules. As a comparison, Si PV modules using passive emitter and rear cell (PERC) are \$0.37/W.[24]

It is clear from Figure 1b that the current synthesis protocol for $CsPbI_3$ QDs (Y = 12%) is not scalable, with \$/m^2 reaching >50. The cost is dominated by materials required for QD synthesis, and the bulk of this contribution comes from the solvents: MeOAc, ODE, and hexane. Labor costs and CapEx in combination form another major contributor. An increase in Y is found to have a dramatic effect, and \$/m^2 approaches 10 at Y = 50%, a yield scenario similar to a recent demonstration.[11] Further increase in Y drops the cost further down to <\$10/m^2. Y as high as 75% has been reported earlier for lead sulfide (PbS) QDs using continuous-flow synthesis.[25] Figure 1c lists strategies for increasing Y.

Impact of Economies-of-Scale (EoS). When computing materials costs for a pilot manufacturing facility, it is important to include EoS considerations that offer discounts on bulk purchases. Here we assumed that the precursors and solvents are purchased in bulk quantities for a 3-month supply. This 3-month supply scales with the target annual coated area. Figure 2a shows the \$/m^2 as a function of annual coated area with EoS considerations for various Y scenarios. Production volumes (megawatts, MW) are also shown, considering these films deliver 20% PCE solar modules. A 20% price discount scenario for every 10× increase in materials purchase volume is shown. Vendor data for bulk purchases based on price quotes and interviews with materials suppliers are included to compare with the learning curve. Detailed discussions on incorporating EoS in the cost model, with illustration Tables S2–S7, are available in the SI.

EoS is found to significantly reduce the costs. Catalog prices from Figure 1b representing 0% discounts are included as ★ for a direct comparison. Higher production volumes (2000 MW) are slightly more cost-effective than 100 MW and lower. The realistic scenario of Y = 50% for a production volume of 2000 MW leads to a \$/m^2 approaching 9, considering vendor rates. Although vendor data approach the 20% discount learning curves for low production volumes around 100 MW, they plateau thereafter. This happens because larger purchases are expected to include extra costs due to shipment, special packaging, etc., resulting in the plateau. For Y = 50%, a 2000 MW annual production volume will require 20,000 kg of PbI_2, 2,920,000 L of MeOAc, and 1,080,000 L of ODE, in addition to the other materials. Purchase, handling, and delivery of such large volumes can involve extra costs that can result in discounts <20%. Figure S1d shows materials requirements for various Y scenarios, which decrease with increasing Y. Materials requirements for various target substrate areas or annual PV production volumes are also shown (Figure S1b,c).

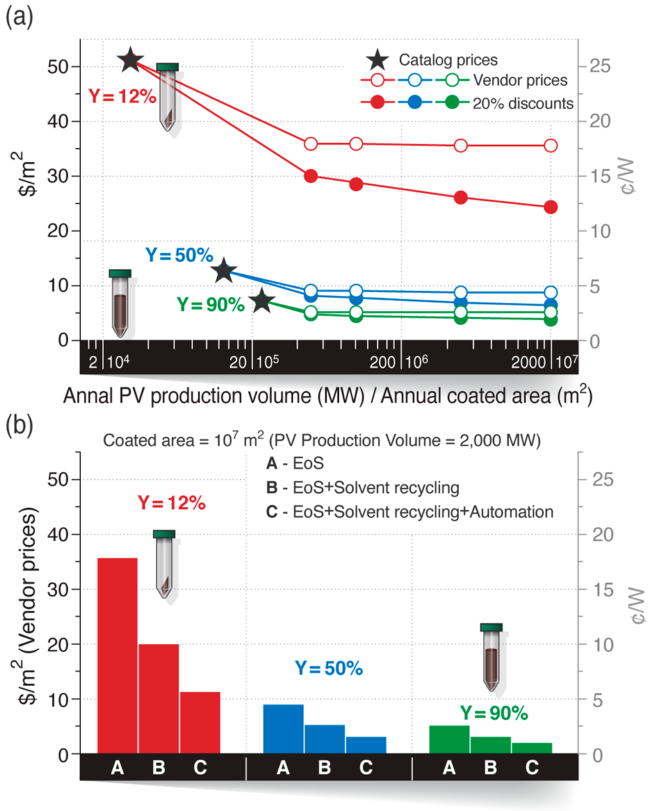

Figure 2. Effects of EoS, solvent recycling, and synthesis automation. (a) Effect of EoS considering vendor price data (open circles) and a 20% discount scenario (solid circles). ★ represents catalog prices from Figure 1. (b) Effects of EoS, solvent recycling, and automation for a coated area of 10^7 m^2, which corresponds to 2000 MW PV annual production volume. Various yield scenarios (red, 12%; blue, 50%; green, 90%) are shown. Vendor prices are considered for the cost of precursors and solvents in this panel.

Impact of Solvent Recycling and Automation. The above calculations have considered that the synthesis protocol and equipment do not change considerably from what is typically followed in a laboratory setup. We now consider a modification to the current PQD purification protocol. Since ODE, MeOAc, and hexane form the major materials cost contributors (Figure 1b) and solvent disposal is a major contributor to CapEx (Tables S3, S5, and S7), we equip the model pilot line with solvent recycling units. The units have a solvent recovery of 90% and recycling capability of 40 L in 24 h, as per information provided by the vendor (see related discussion in the SI). This introduces a 90% reduction in the requirements of ODE, MeOAc, and hexane and removes the costs associated with solvent disposal. Figure 2b (bars B) shows the effect of this step, considering an annual production volume of 2000 MW. For $Y = 50\%$, the $/m^2 drops from 9 to 5, and to 3 for $Y = 90\%$.

A combination of higher Y and solvent recycling can clearly lead to market-compatible QD synthesis. We were interested in seeing if further cost-lowering factors can be introduced such that even the low Y scenarios (~50%) can become cost-effective. For this we simulated the scenario of QD synthesis automation. Briefly, this was done either by considering reduced labor rates or by reducing the equipment-to-employee ratio. Both scenarios represent reduced human intervention and are detailed in the SI.

For labor rate reduction, a rate of $1/h was considered compared to a U.S. standard rate of $27/h. Since automation is less cost intensive, this reduction can imply minimal human intervention, amounting to a significantly reduced labor charge. This can also represent synthesis in a lower wage country where labor rates can be as low as $1/h. As Figure 2b highlights (bars C), $/m^2 is found to decrease below 3 for $Y = 50\%$. Interestingly, a more prominent cost reduction is observed for $Y = 12\%$, suggesting that automation helps lower Y scenarios more prominently and might not be needed if the pilot line can operate at $Y = 50\%$ or higher.

In the second approach, automation was simulated by reducing the equipment-to-employee ratio from 1:1 to 10:1, since artificial intelligence enabled smart manufacturing is expected to be significantly less labor-intensive. Standard U.S. labor rates were considered. An automated platform has recently been demonstrated for PQD synthesis with machine-learning algorithms to guide the process.[26] Results are shown in Figure S2 and enable a level of cost reduction similar to that of the reduced labor rate scenario.

Future Research Directions. The cost analysis presented here illustrates the case of $CsPbI_3$ PQDs synthesized using the hot-injection method. Using this structure, other PQD compositions of interest can be similarly modeled. As the next step, this analysis should be extended to the R2R and sheet-to-sheet coating stage and will involve determining the most cost-effective coating technique while maintaining a high coating speed. While we expect most large-area industrial-compatible coating techniques to contribute negligibly to $/m^2 from a CapEx, OpEx, and labor cost perspective, only a few coating techniques can allow high coating throughput. Modeling an automated coating system can be challenging since such a technique has not yet been industrially demonstrated.

Based on insights from this cost-model, we present below key future research directions for industry-compatible PQD optoelectronics:

I. *Modified chemical synthesis.* PQD synthesis should be explored with reaction volumes of 1 L and higher, beyond the current laboratory standard of 25 mL. Synthesis methods that require lower Pb:Cs precursor ratio and suppress PbI_2 wastage should be studied. It is equally important to understand the impact of lower-grade solvents and precursors, and solvent recycling, on the PQD synthesis yield and quality. Replacing costly ODE with a lower boiling point solvent, such as ethylene glycol, can drive the cost down further.

II. *Scalable fabrication of PQDs and stable optoelectronic devices.* Flow synthesis of PQDs offers ease of scale-up without batch-to-batch variations,[26] and demonstrating high-performance optoelectronic devices using these lower-cost PQDs is crucial to industrial scale-up. R2R coating and scalable fabrication of large-area PQD films should be explored for agrivoltaics and large-area display applications.[19,27] Achieving long-term PQD device stability should be an important goal. While inorganic PQDs intrinsically offer greater phase stability due to lattice strain,[6] robust chemical and mechanical encapsulation schemes and packaging designs need to be explored to meet industrial stability standards.

III. *Quantifying environmental impact.* Finally, it is critical to establish the environmental impact of PQD optoelectronics by quantifying the carbon footprint, in particular, for agrivoltaics applications.[28] Greener alternatives for processing solvents should be screened by performing a disability-adjusted life year (DALY) analysis.[29] Moving toward greener alternatives is also expected to allow cost reductions.[30]

In summary, a comprehensive technoeconomic cost analysis of perovskite quantum dot optoelectronics is reported. Using economies-of-scale considerations based on price data from prominent materials suppliers, we have highlighted that increased QD synthesis yield, solvent recycling, and synthesis automation are critical to market adoption of this technology. In combination, this three-pronged approach can drive quantum dot film fabrication costs down from >$50/m^2 to ~$2−3/m^2.

Ahmad R. Kirmani orcid.org/0000-0002-8351-3762
Michael Woodhouse
Joseph M. Luther orcid.org/0000-0002-4054-8244

ASSOCIATED CONTENT

Supporting Information

The Supporting Information is available free of charge at https://pubs.acs.org/doi/10.1021/acsenergylett.2c00250.

Detailed explanation of the cost model with cost tables, $/m^2 for automation, substrate area, and materials required vs production volume (PDF)

AUTHOR INFORMATION

Complete contact information is available at:
https://pubs.acs.org/10.1021/acsenergylett.2c00250

Notes

Views expressed in this Energy Focus are those of the authors and not necessarily the views of the ACS.
The authors declare no competing financial interest.
The views expressed in the article do not necessarily represent the views of the DOE or the U.S. Government.

ACKNOWLEDGMENTS

This work was authored by the National Renewable Energy Laboratory, operated by Alliance for Sustainable Energy, LLC, for the U.S. Department of Energy (DOE) under Contract No. DE-AC36-08GO28308. The authors acknowledge support from Solar Energy Technologies Office of DOE.

REFERENCES

(1) Kirmani, A. R.; et al. Colloidal Quantum Dot Photovoltaics: Current Progress and Path to Gigawatt Scale Enabled by Smart Manufacturing. *ACS Energy Lett.* **2020**, *5* (9), 3069−3100.

(2) Parrish, C. H.; et al. Optimizing spectral quality with quantum dots to enhance crop yield in controlled environments. *Commun. Biol.* **2021**, *4* (1), 124.

(3) Dey, A.; et al. State of the Art and Prospects for Halide Perovskite Nanocrystals. *ACS Nano* **2021**, *15* (7), 10775−10981.

(4) Hao, M.; et al. Ligand-assisted cation-exchange engineering for high-efficiency colloidal $Cs_{1-x}FA_xPbI_3$ quantum dot solar cells with reduced phase segregation. *Nat. Energy* **2020**, *5* (1), 79−88.

(5) Zhao, Q.; et al. High efficiency perovskite quantum dot solar cells with charge separating heterostructure. *Nat. Commun.* **2019**, *10* (1), 2842.

(6) Swarnkar, A.; et al. Quantum dot-induced phase stabilization of α-$CsPbI_3$ perovskite for high-efficiency photovoltaics. *Science* **2016**, *354* (6308), 92−95.

(7) Protesescu, L.; et al. Nanocrystals of Cesium Lead Halide Perovskites ($CsPbX_3$, X = Cl, Br, and I): Novel Optoelectronic Materials Showing Bright Emission with Wide Color Gamut. *Nano Lett.* **2015**, *15* (6), 3692−3696.

(8) Kirmani, A. R. Commercializing colloidal quantum dot photovoltaics. *MRS Bull.* **2019**, *44* (7), 524−525.

(9) Wheeler, L. M.; et al. Targeted Ligand-Exchange Chemistry on Cesium Lead Halide Perovskite Quantum Dots for High-Efficiency Photovoltaics. *J. Am. Chem. Soc.* **2018**, *140* (33), 10504−10513.

(10) Sanehira, E. M.; et al. Enhanced mobility $CsPbI_3$ quantum dot arrays for record-efficiency, high-voltage photovoltaic cells. *Sci. Adv.* **2017**, *3* (10), No. eaao4204.

(11) Wang, Y.; et al. Surface Ligand Management Aided by a Secondary Amine Enables Increased Synthesis Yield of $CsPbI_3$ Perovskite Quantum Dots and High Photovoltaic Performance. *Adv. Mater.* **2020**, *32* (32), 2000449.

(12) Lignos, I.; et al. Synthesis of Cesium Lead Halide Perovskite Nanocrystals in a Droplet-Based Microfluidic Platform: Fast Parametric Space Mapping. *Nano Lett.* **2016**, *16* (3), 1869−1877.

(13) Maceiczyk, R. M.; et al. Microfluidic Reactors Provide Preparative and Mechanistic Insights into the Synthesis of Formamidinium Lead Halide Perovskite Nanocrystals. *Chem. Mater.* **2017**, *29* (19), 8433−8439.

(14) Cho, S.; et al. High-Voltage and Green-Emitting Perovskite Quantum Dot Solar Cells via Solvent Miscibility-Induced Solid-State Ligand Exchange. *Chem. Mater.* **2020**, *32* (20), 8808−8818.

(15) Kirmani, A. R.; et al. Optimizing Solid-State Ligand Exchange for Colloidal Quantum Dot Optoelectronics: How Much Is Enough? *ACS Appl. Energy Mater.* **2020**, 3 (6), 5385−5392.

(16) Chuang, C.-H. M.; et al. Improved performance and stability in quantum dot solar cells through band alignment engineering. *Nat. Mater.* **2014**, *13* (8), 796−801.

(17) Kirmani, A. R.; et al. Effect of Solvent Environment on Colloidal-Quantum-Dot Solar-Cell Manufacturability and Performance. *Adv. Mater.* **2014**, *26* (27), 4717−4723.

(18) Lu, K.; et al. High-Efficiency PbS Quantum-Dot Solar Cells with Greatly Simplified Fabrication Processing via "Solvent-Curing. *Adv. Mater.* **2018**, *30* (25), 1707572.

(19) Kirmani, A. R.; et al. Overcoming the Ambient Manufacturability-Scalability-Performance Bottleneck in Colloidal Quantum Dot Photovoltaics. *Adv. Mater.* **2018**, *30* (35), 1801661.

(20) Sukharevska, N.; et al. Scalable PbS Quantum Dot Solar Cell Production by Blade Coating from Stable Inks. *ACS Appl. Mater. Interfaces* **2021**, *13* (4), 5195−5207.

(21) Aqoma, H.; et al. Solid-state-ligand-exchange free quantum dot ink-based solar cells with an efficiency of 10.9%. *Energy Environ. Sci.* **2018**, *11* (6), 1603−1609.

(22) Jean, J.; et al. Accelerating Photovoltaic Market Entry with Module Replacement. *Joule* **2019**, 3 (11), 2824−2841.

(23) Rolston, N.; et al. Rapid Open-Air Fabrication of Perovskite Solar Modules. *Joule* **2020**, *4* (12), 2675−2692.

(24) Woodhouse, M.; et al. Crystalline Silicon Photovoltaic Module Manufacturing Costs and Sustainable Pricing: 1H 2018 Benchmark and Cost Reduction Road Map. National Renewable Energy Laboratory (NREL): Golden, CO, 2019.

(25) Pan, J.; et al. Automated Synthesis of Photovoltaic-Quality Colloidal Quantum Dots Using Separate Nucleation and Growth Stages. *ACS Nano* **2013**, *7* (11), 10158−10166.

(26) Epps, R. W.; et al. Artificial Chemist: An Autonomous Quantum Dot Synthesis Bot. *Adv. Mater.* **2020**, *32* (30), No. e2001626.

(27) Deng, Y.; et al. Surfactant-controlled ink drying enables high-speed deposition of perovskite films for efficient photovoltaic modules. *Nat. Energy* **2018**, *3* (7), 560−566.

(28) Tian, X.; et al. Life cycle energy use and environmental implications of high-performance perovskite tandem solar cells. *Sci. Adv.* **2020**, *6* (31), No. eabb0055.

(29) Vidal, R.; et al. Assessing health and environmental impacts of solvents for producing perovskite solar cells. *Nat. Sustain.* **2021**, *4* (3), 277−285.

(30) Swartwout, R.; et al. Predicting Low Toxicity and Scalable Solvent Systems for High-Speed Roll-to-Roll Perovskite Manufacturing. *Solar RRL* **2021**, 2100567.